International Journal for Uncertainty Quantification, 3 (2): 101–117 (2013)

APPROXIMATE LEVEL-CROSSING PROBABILITIES FOR INTERACTIVE VISUALIZATION OF UNCERTAIN ISOCONTOURS

Kai Pöthkow, Christoph Petz, & Hans-Christian Hege*

Zuse Institute Berlin, Takustrasse 7, 14195 Berlin, Germany

Original Manuscript Submitted: 09/02/2011; Final Draft Received: 07/12/2012

A major method for quantitative visualization of a scalar field is depiction of its isocontours. If the scalar field is afflicted with uncertainties, uncertain counterparts to isocontours have to be extracted and depicted. We consider the case where the input data is modeled as a discretized Gaussian field with spatial correlations. For this situation we want to compute level-crossing probabilities that are associated to grid cells. To avoid the high computational cost of Monte Carlo integrations and direction dependencies of raycasting methods, we formulate two approximations for these probabilities that can be utilized during rendering by looking up precomputed univariate and bivariate distribution functions. The first method, called maximum edge crossing probability, considers only pairwise correlations at a time. The second method, called linked-pairs method, considers joint and conditional probabilities between vertices along paths of a spanning tree over the n vertices of the grid cell; with each possible tree an n-dimensional approximate distribution is associated; the choice of the distribution is guided by minimizing its Bhattacharyya distance to the original distribution. We perform a quantitative and qualitative evaluation of the approximation errors on synthetic data and show the utility of both approximations on the example of climate simulation data.

KEY WORDS: *scalar fields, spatial uncertainty, level-crossing probabilities, approximation, visualization*

1. INTRODUCTION

Data acquired by measurements or simulations are always affected by uncertainty. Important sources of uncertainty include the measurement process, parameter selection, discretization and quantization of continuous quantities, as well as numerical simulations with finite precision. Modeling and visualization techniques taking care of uncertainties therefore are of interest for a variety of applications. In this paper we revisit the extraction of uncertain counterparts to isocontours.

In previous work we have proposed a method to compute level-crossing probabilities for cells in Gaussian fields defined on grids, considering the spatial correlation structure of the input data [1]. A disadvantage of this approach is the high computational cost of the Monte Carlo (MC) integration. For the specific case of Gaussian fields with exponential correlation functions, Pfaffelmoser et al. [2] presented a raycasting approach that computes first-crossing probabilities along rays using lookup tables for fast evaluation. The results of this method depend on the viewing direction.

Our aim is to improve the computation of local cellwise level-crossing probabilities that arise from *arbitrary* spatial correlations and that are independent of the viewing direction, i.e., are objective, in the sense that they are independent of the observer. Since the input data are usually given on some grid, it is a natural choice to consider grid cells and to compute cell-related probabilities.

The numerical computation of high-dimensional integrals in general is expensive, both with deterministic and MC methods. There are two ways to deal with this problem: Either utilize specific properties of the problem to facilitate the computation, or find good and fast approximations of the integrals. Here we consider the latter approach: We

*Correspond to Kai Pöthkow, E-mail: poethkow@zib.de, URL: http://www.zib.de/visual

2152–5080/13/$35.00

compute approximate univariate and bivariate distribution functions that can be evaluated in the rendering step using table lookups.

We will consider two possibilities for approximating the probabilities. The *maximum edge crossing method* considers pairwise correlations between two random variables at a time. The *linked-pairs method* iteratively traverses the vertices of a grid cell and considers joint and conditional probabilities between subsequent vertices. This algorithm induces an n-dimensional approximate distribution, where n is the number of vertices. Depending on the order in which the vertices are traversed, different approximate probability distributions occur; an optimal distribution is selected by optimizing the Bhattacharyya distance to the original distribution.

The main contributions of this paper are

- a formulation of two approximations for cellwise level-crossing probabilities in discretized Gaussian fields with arbitrary spatial correlations,
- an optimization strategy for approximate probability distributions based on the Bhattacharyya distance,
- and a quantitative and qualitative evaluation of the approximation errors for synthetic data and climate simulation results.

2. RELATED WORK

Johnson and Sanderson [3] considered the representation of uncertainty to be a major challenge in visualization research. An earlier introduction to uncertainty visualization describing various aspects of uncertainty propagation and several visualization methods was presented by Pang et al. [4].

In several different areas of visualization, research methods to represent data uncertainty have been proposed. The visualization of ensemble data was addressed by Potter et al. [5] and Sanyal et al. [6]. Both papers present visualization tools for weather forecasts and simulated climate data. Sanyal et al. also conducted an evaluation of their tool's efficiency. Luo et al. [7] described methods to manipulate ensemble data, assess uncertainty propagation, and adapt specific visualization methods. Methods to display uncertain data using volume rendering include special transfer functions that take mean values and variances into account [8], interactive probabilistic classification [9], and animation of probabilistic transfer functions [10]. Visualizations of uncertain vector field and flow data can be created using specific texture mapping approaches [11] or the application of an extension of vector field topology [12].

The uncertainty of the positions and shapes of surfaces was addressed in several publications. Pauly et al. [13] quantified the uncertainty of surface reconstructions from point cloud data using likelihood and confidence maps. Grigoryan and Rheingans [14] indicated the positional uncertainty of surfaces using point primitives that are displaced in the normal direction of the mean surfaces. Zehner et al. [15] proposed to combine isosurfaces with additional geometry to indicate the positional uncertainty in geological data and show spatial confidence intervals.

Allendes Osorio and Brodlie [16] modeled the uncertainty of scalar fields using random fields. To display spatial distributions of uncertain isolines they computed the probability that the scalar value at a given position is contained in an interval between an isovalue and a second user-defined parameter. Pöthkow and Hege [17] estimated the sensitivity of isocontours using the numerical condition, displayed it using color mapping, and plotted average condition numbers to aid the selection of isovalues corresponding to robust/insensitive surfaces. As a model for uncertain scalar fields they used discrete random fields and proposed an interpolation scheme. To compute spatial distributions of uncertain isocontours and isosurfaces they defined local measures for each point in a continuous domain and displayed the results by volume rendering that was combined with crisp mean surfaces.

One drawback of the above approaches was that spatial correlations in the random fields were not considered. Both Pfaffelmoser et al. [2] and Pöthkow et al. [1] proposed methods to incorporate covariances in Gaussian random fields to compute more accurate level-crossing probabilities. In [2] a formulation of first-crossing probabilities in fields with exponential correlation functions was presented which uses lookup tables for fast evaluation. It was employed in a real-time volume raycasting algorithm and combined with specific surface rendering and coloring methods. In [1] covariances were considered for the computation of level-crossings in each cell of a discretized random field. The probabilities were estimated using MC integration.

3. MATHEMATICAL MODEL

We consider a scalar field $g : M \to \mathbb{R}$ on a compact domain $M \subset \mathbb{R}^d$ that has been discretely sampled on nodes $\{\mathbf{x}\}_{i\in I}$ of a grid with data values $\{Y\}_{i\in I}$, where $I = \{1, \ldots, l\}$ labels the sample points. To refer to grid entities such as nodes, edges, faces, and volume cells, we use the term η-*cell*: a 0-cell is a *vertex*, a 1-cell is an *edge*, a 2-cell is a *polygon*, a 3-cell is a *polyhedron*, and so on. The sampling grid is a d-dimensional grid composed of d-cells that discretizes a d-dimensional geometric domain in $\mathbb{R}^d$.

3.1 Basic Probabilistic Setting

We assume that the data values $\{Y\}_{i\in I}$ at the sampling points $\{\mathbf{x}\}_{i\in I}$ are random variables with probability density distributions f_i, means $\mu_i = \mathrm{E}(Y_i)$, finite variances $\sigma_i^2 = \mathrm{E}(Y_i - \mu_i)^2$, and covariances $\mathrm{Cov}(Y_i, Y_j) = \mathrm{E}[(Y_i - \mu_i)(Y_j - \mu_j)]$ for all $i, j \in I$.

Given N realizations of the random field $\{y\}_{i\in I}^{j=1,\ldots N}$, i.e., a sample of random fields, the sample means (or empirical means) $\hat{\mu}_i = \frac{1}{N}\sum_{k=1}^{N} y_i^k$ and the entries of the sample covariance matrix $\widehat{\mathrm{Cov}}_{i,j} = \frac{1}{N-1}\sum_{k=1}^{N}(y_i^k - \hat{\mu}_i)(y_j^k - \hat{\mu}_j)$ for all $i, j \in I$ are unbiased estimates of the means $\mathrm{E}(Y_i)$ and covariances $\mathrm{Cov}(Y_i, Y_j)$, respectively.

3.2 Joint Distribution Functions

For a vector $\mathbf{Y}$ of n random variables $\{Y\}_{i\in I}$ the variances and covariances can be represented by a positive-semidefinite covariance matrix

$$\Sigma = (\mathrm{Cov}(Y_i, Y_j))_{1\le i,j\le n}.$$

In case $\mathbf{Y}$ conforms to a multivariate Gaussian distribution $\mathbf{Y} \sim \mathcal{N}_n(\mu, \Sigma)$ with $\mu = [\mathrm{E}(Y_1), \mathrm{E}(Y_2), \ldots, \mathrm{E}(Y_n)]^T$, it can be uniquely described by a joint probability density function

$$f_{\mathbf{Y}}(\mathbf{y}) = \frac{1}{(2\pi)^{n/2}\det(\Sigma)^{1/2}} \exp\left[-\tfrac{1}{2}(\mathbf{y}-\mu)^T\Sigma^{-1}(\mathbf{y}-\mu)\right]$$

with $\mathbf{y} \in \mathbb{R}^n$.

3.3 Level-Crossing Probabilities

Any realization $\{y\}_{i\in I}$ of $\mathbf{Y}$ defines a grid function. For any grid function imagine an extension to a C^0 function $g_{\{y\}}$ that is defined in the continuous domain and that interpolates between the sample points $\{\mathbf{x}_i\}_{i\in I}$ such that in each η–cell c ($\eta \le d$) the extremal values are taken at the vertices of c. Examples for such interpolations are linear interpolation for simplicial cells and η–linear interpolation for η–dimensional cubical cells.

Let $\tilde{I} \in I$ be the set of indices of the vertices of cell c. Then cell c crosses the ϑ-level of $g_{\{y\}}$ if and only if in the set of differences $(y_i - \vartheta)_{i\in\tilde{I}}$ both signs occur. Equivalently, cell c does not cross the ϑ-level of $g_{\{y\}}$, if and only if all differences $(y_i - \vartheta)_{i\in\tilde{I}}$ have the same sign.

We want to compute the probability that a η-cell c of the d-dimensional sample grid ($\eta \le d$) crosses the ϑ-level of interpolated realizations of the random variables $\{Y\}_{i\in I}$. We call this the ϑ-*level-crossing probability* of cell c and denote it by $\mathrm{P}_c(\vartheta\text{-crossing})$. In order to compute this probability we have to integrate the joint density function of the random variables $\{Y\}_{i\in\tilde{I}}$ over sets $\{y_i \in \mathbb{R} \,|\, y_i \le \vartheta\}$ and $\{y_j \in \mathbb{R} \,|\, y_j \ge \vartheta\}$ using integrals over $|\tilde{I}|$-dimensional marginal density functions.

In general, marginalizing out the other variables $\{Y\}_{i\notin\tilde{I}}$ can be difficult. However, for multivariate Gaussian distributions we can utilize the nice property that marginalized distributions are again Gaussian distributions with the "right" means and covariances, i.e., the rows and columns of μ and Σ that correspond to $\{Y\}_{i\notin\tilde{I}}$ are deleted to obtain the local marginal distribution of $\{Y\}_{i\in\tilde{I}}$; see [1].

As an alternative to the direct formulation we can also compute the probability

$$\mathrm{P}_c(\vartheta\text{-crossing}) = 1 - \mathrm{P}_c(\vartheta\text{-noncrossing})\,, \tag{1}$$

which in cells of dimension greater than 1 is less expensive to calculate.

The general procedure to compute such probabilities can be applied to any type of mesh entity, for example, to arbitrary polyhedral cells in grids of arbitrary dimension d. In the following we consider exemplarily edges of such grids. Obviously the procedure can be extended to η-simplices or arbitrary η-polyhedra with $\eta \leq d$.

3.3.1 Edges

For a scalar field in one or more dimensions we consider two random variables Y_1, Y_2 that are associated with adjacent grid points x_1, x_2. Consider the random vector $\mathbf{Y} = [Y_1, Y_2]$ where the joint probability distribution is described by a bivariate Gaussian probability density function (PDF) $f_{\mathbf{Y}}(y_1, y_2)$ with $y_1, y_2 \in \mathbb{R}$. We define the events $Y_i^+ = (Y_i > \vartheta)$ and $Y_i^- = (Y_i \leq \vartheta)$. The ϑ-level-crossing probability is given by

$$\begin{aligned} \mathrm{P}_c(\vartheta\text{-crossing}) &= \mathrm{P}(Y_1^- \cap Y_2^+) \;+\; \mathrm{P}(Y_1^+ \cap Y_2^-) \\ &= \int\limits_{y_1 \leq \vartheta} \mathrm{d}y_1 \int\limits_{y_2 > \vartheta} \mathrm{d}y_2 \; f_{\mathbf{Y}}(y_1, y_2) + \int\limits_{y_1 > \vartheta} \mathrm{d}y_1 \int\limits_{y_2 \leq \vartheta} \mathrm{d}y_2 \; f_{\mathbf{Y}}(y_1, y_2). \end{aligned} \tag{2}$$

Alternatively:

$$\begin{aligned} \mathrm{P}_c(\vartheta\text{-non-crossing}) &= \mathrm{P}(Y_1^- \cap Y_2^-) \;+\; \mathrm{P}(Y_1^+ \cap Y_2^+) \\ &= \int\limits_{y_1 \leq \vartheta} \mathrm{d}y_1 \int\limits_{y_2 \leq \vartheta} \mathrm{d}y_2 \; f_{\mathbf{Y}}(y_1, y_2) + \int\limits_{y_1 > \vartheta} \mathrm{d}y_1 \int\limits_{y_2 > \vartheta} \mathrm{d}y_2 \; f_{\mathbf{Y}}(y_1, y_2). \end{aligned} \tag{3}$$

Since the four quadrants $\{(y_1, y_2) | y_1 \leq \vartheta \text{ and } y_2 \leq \vartheta\}$, $\{(y_1, y_2) | y_1 \leq \vartheta \text{ and } y_2 > \vartheta\}$, $\{(y_1, y_2) | y_1 > \vartheta \text{ and } y_2 \leq \vartheta\}$ and $\{(y_1, y_2) | y_1 > \vartheta \text{ and } y_2 > \vartheta\}$ are disjoint and their union is $\mathbb{R}^2$ we can read off Eq. (1).

3.3.2 Computing the Bivariate Probability Integral

The edge-level-crossing probability as given in Eq. (3) depends on the parameters μ_1, μ_2, $\mathrm{Cov}_{1,1}$, $\mathrm{Cov}_{2,2}$, $\mathrm{Cov}_{1,2}$ and ϑ. The integral can be expressed in terms of the *standard normal* cumulative distribution function $\Phi(y_1, y_2, \rho)$, with *correlation coefficient* $\rho = \frac{\mathrm{Cov}_{1,2}}{\sigma_1 \, \sigma_2}$, standard deviation $\sigma_i = \sqrt{\mathrm{Cov}_{i,i}}$ and integration bounds given by the *stochastic distance function*

$$\Psi_i = \frac{\mu_i - \vartheta}{\sigma_i},$$

such that

$$\begin{aligned} \mathrm{P}_c(\vartheta\text{-crossing}) &= 1 - \big(\mathrm{P}(Y_1 \leq \vartheta, Y_2 \leq \vartheta) + \mathrm{P}(Y_1 > \vartheta, Y_2 > \vartheta)\big) \\ &= 1 - \big(\Phi(-\Psi_1, -\Psi_2, \rho) + \Phi(\Psi_1, \Psi_2, \rho)\big). \end{aligned} \tag{4}$$

This is a very convenient formulation because $\Phi(y_1, y_2, \rho)$ can be efficiently evaluated using a 3D lookup table [2].

3.3.3 Level-Crossing in Higher Dimensions

For a scalar field in two or more dimensions we consider $\mathbf{Y} = [Y_1, Y_2, \ldots, Y_n]$ at the grid points $\mathbf{x}_1, \mathbf{x}_2, \ldots, \mathbf{x}_n$ which are the corners of cell with n vertices; see Fig. 1 for an example. The joint probability distribution is described by an n-dimensional Gaussian PDF $f_{\mathbf{Y}}(y_1, y_2, \ldots, y_n)$ with $y_1, y_2, \ldots, y_n \in \mathbb{R}$.

According to Eq. (1), the level-crossing probability for a cell can be computed by considering the *complement* of the cases where *no* level-crossing occurs by

$$\mathrm{P}_c(\vartheta\text{-crossing}) = 1 - \big[\mathrm{P}(Y_1^- \cap Y_2^- \ldots \cap Y_n^-) + \mathrm{P}(Y_1^+ \cap Y_2^+ \ldots \cap Y_n^+)\big]. \tag{5}$$

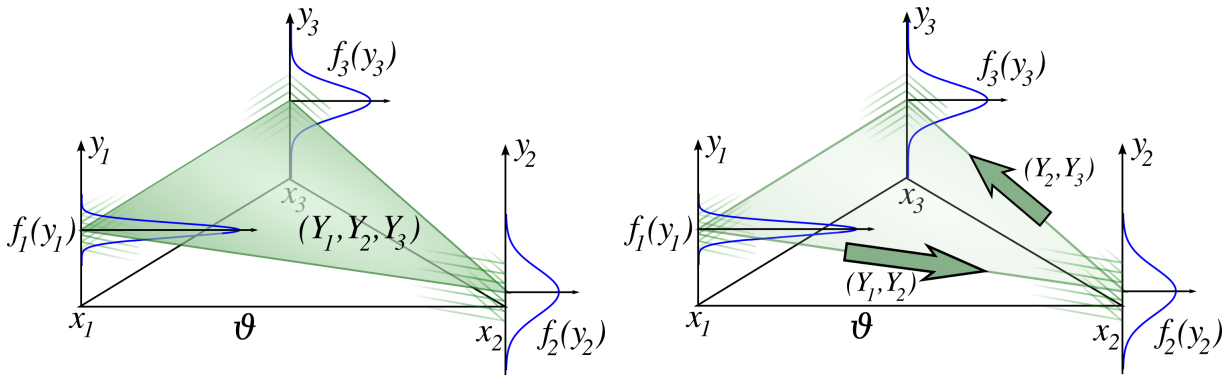

FIG. 1: Example for the computation of a level-crossing probability in a triangular cell. The marginal distributions at the grid points are shown in blue. Exemplarily, one realization of the interpolant is shown in green. (a) corresponds to the consideration of the complete covariance matrix in Eq. (5) while (b) shows the approximation using pairwise correlations in Eq. (11).

Thus, n-dimensional integral expressions such as

$$\mathrm{P}(Y_1^+ \cap Y_2^+ \ldots \cap Y_n^+) = \int\limits_{y_1>\vartheta} \mathrm{d}y_1 \int\limits_{y_2>\vartheta} \mathrm{d}y_2 \ \ldots \int\limits_{y_n>\vartheta} \mathrm{d}y_n \ f_{\mathbf{Y}}(y_1, y_2, \ldots, y_n) \tag{6}$$

need to be evaluated. In general, these integrals cannot be evaluated in closed form. Numerical integration schemes, e.g., Monte Carlo methods, can be used for estimation.

4. APPROXIMATE LEVEL-CROSSING PROBABILITIES

To allow fast interactive visualization, expensive numerical integration must be avoided. In addition to the trivial approach that simply neglects the correlation structure we propose two *approximations* for level-crossing probabilities that can be evaluated very efficiently, but consider correlations. The methods we define and compare in the following are (i) the vertex-centered method assuming statistical independence, (ii) the maximum edge crossing probability, and (iii) the linked-pairs approximation method.

4.1 Vertex- and Edge-Centered Approximation Strategies

4.1.1 Statistically Independent Vertices

The first, highly simplified approach completely neglects the correlation structure and computes probabilities under the assumption that all random variables are statistically independent. The level-crossing probability for cell c is then

$$\mathrm{Q}_c = 1 - \left[\mathrm{P}(Y_1^+)\mathrm{P}(Y_2^+)\ldots\mathrm{P}(Y_n^+) + \mathrm{P}(Y_1^-)\mathrm{P}(Y_2^-)\ldots\mathrm{P}(Y_n^-)\right]. \tag{7}$$

However, this way the spatial distribution of uncertain isocontours is often overestimated [1, 2].

4.1.2 Maximum Edge Crossing Probability

The second measure to approximate the cell-level-crossing probability is the maximum edge-level-crossing probability over all edges. Taking spatial correlations into account, the smallest grid entity to consider is an edge that connects any two points (Y_1, Y_2) of a cell. If a cell with n vertices and m edges contains a level-crossing, at least one of its edges contains a level-crossing as well. The converse is obviously true as well: As soon as a level-crossing occurs between

any two vertices, the cell has a level-crossing. Thus, the edgewise level-crossing probability is a lower bound for the cell integral. As an approximation for the cellwise level-crossing probability, we use the maximum lower bound, e.g.,

$$\mathrm{R}_c = \max_{i=1\ldots m} \left\{1 - \left[\mathrm{P}(Y_{i,1}^+ \cap Y_{i,2}^+) + \mathrm{P}(Y_{i,1}^- \cap Y_{i,2}^-)\right]\right\}, \tag{8}$$

where $Y_{i,1}$ and $Y_{i,2}$ are the random variables associated with the vertices that are connected by edge i. In other words, we reduce the n-dimensional distribution to two-dimensional (2D) marginal distributions to find the edge with maximum level-crossing probability.

To get an intuition why the edgewise level-crossing probability is indeed a lower bound consider the example of a single triangular cell with independent Gaussian distributions at the vertices $Y_{1,2,3} \sim \mathcal{N}(0,1)$. For the isovalue $\vartheta = 0$, the maximum edge crossing probability is $\mathrm{R}_c = 0.5$. In contrast, the cellwise crossing probability is $\mathrm{P}_c = 1 - [\mathrm{P}(Y_1^+ \cap Y_2^+ \cap Y_3^+) + \mathrm{P}(Y_1^- \cap Y_2^- \cap Y_3^-)] = 0.75$. Generally, for cells with $n > 2$ vertices the cellwise crossing probability is larger or equal to the maximum edgewise probability because a crossing may also occur on other edges than the one corresponding to the maximum crossing probability.

4.2 Linked-Pairs Approximation

For the third approximation, more correlations are considered. Both 2D joint and conditional probabilities for level-crossings between any two variables of a cell can be evaluated using lookup tables. To exploit that, pairwise conditional probabilities are evaluated in a step by step fashion from vertex to vertex of a cell; see Fig. 1. We show that this method induces an approximate distribution that is again normally distributed. The approach has a degree of freedom in the choice of the traversal order of the vertices $\{\mathbf{x}_1, \mathbf{x}_2, \ldots, \mathbf{x}_n\}$ that can be described by a spanning tree. The Bhattacharyya distance is used to compare the different choices to the original distribution.

4.2.1 Approximate Probabilities

We approximate $\mathrm{P}(Y_1^+ \cap Y_2^+ \ldots \cap Y_n^+)$ by

$$\tilde{\mathrm{P}}(Y_1^+, Y_2^+, \ldots, Y_n^+) \;:=\; \mathrm{P}(Y_1^+ \cap Y_2^+)\, \mathrm{P}(Y_3^+ | Y_2^+) \;\ldots\; \mathrm{P}(Y_n^+ | Y_{n-1}^+) \tag{9}$$

with conditional probabilities

$$\mathrm{P}(Y_i^+ | Y_{i-1}^+) \;=\; \frac{\mathrm{P}(Y_{i-1}^+ \cap Y_i^+)}{\mathrm{P}(Y_{i-1}^+)}.$$

The choice of pairwise joint probabilities that need to be evaluated in Eq. (9) was chosen arbitrarily, but influences the result. The joint probabilities in each term determine which of the pairwise correlations are considered. A natural choice does not exist. To make the choice of pairs of vertices explicit, we reformulate Eq. (9) such that the parameter $k \in \{1, 2, \ldots, n^{n-2}\}$ identifies a spanning tree over all vertices of the cell. The approximate probability is given by

$$\tilde{\mathrm{P}}(Y_1^+, Y_2^+, \ldots, Y_n^+; k) = \mathrm{P}(S_1^k \cap S_2^k)\, \frac{\mathrm{P}(S_3^k \cap S_4^k)}{\mathrm{P}(S_3^k)}\, \frac{\mathrm{P}(S_5^k \cap S_6^k)}{\mathrm{P}(S_5^k)} \ldots \tag{10}$$

where $\{S^1, \ldots, S^{n^{n-2}}\}$ are the n^{n-2} possible *spanning trees* over n vertices, and each tree is given as an edge list $S^k = \{\{S_1^k, S_2^k\}; \{S_3^k, S_4^k\}; \ldots\}$. A method for the optimal choice of k will be derived in the next section. Analogously we can define $\tilde{\mathrm{P}}(Y_1^-, Y_2^-, \ldots, Y_n^-; k)$. The *approximate level-crossing probability* is given by

$$\tilde{\mathrm{P}}_c = 1 - \left[\tilde{\mathrm{P}}(Y_1^+, Y_2^+, \ldots, Y_n^+; k) + \tilde{\mathrm{P}}(Y_1^-, Y_2^-, \ldots, Y_n^-; k)\right]. \tag{11}$$

4.2.2 Approximate Distribution

For the evaluation of the approximation $\tilde{\mathrm{P}}_c$ in Eq. (10) only the pairwise correlations between random variables as given by the spanning tree S^k are used. This algorithm induces a new joint distribution for all variables. Starting from the original Gaussian random vector $\mathbf{Y} \sim \mathcal{N}(\mu, \Sigma)$ of a grid cell c, we derive the approximate distribution and show that the approximated distribution is again a multivariate normal distribution

$$\tilde{\mathbf{Y}} \sim \mathcal{N}(\mu, \tilde{\Sigma}).$$

The expected values are identical for $\mathbf{Y}$ and $\tilde{\mathbf{Y}}$.

The covariance matrix $\tilde{\Sigma}$ that is induced by the approximation is computed as follows: Starting from Y_1 we evaluate the correlations of the cell in a step by step fashion. Traversing the spanning tree S^k from a cell vertex Y_1 gives an ordered list of edges $\{(i,j)\}$. For each edge (i,j) we extend the distribution iteratively with $\rho_{i,j}$ describing the correlation between Y_i and Y_j. Thus, we extend the random vector $\mathbf{Y}$ by Y_i or Y_j, respectively, depending on which one was not already included in a previous step. According to the derivations in the Appendix the correlation coefficients for this distribution are

$$\tilde{\rho}_{i,j} = \rho_{i,j}, \tag{12}$$

and

$$\tilde{\rho}_{\zeta,j} = \tilde{\rho}_{\zeta,i}\rho_{i,j}, \tag{13}$$

where $\zeta \neq i$. After iterating over all edges we can compute $\tilde{\Sigma}$ from the correlation coefficients $\tilde{\rho}_{i,j}$.

In other words, $\tilde{\rho}_{i,j}$ is the product of the correlation coefficients along the path of the spanning tree connecting the variables Y_i and Y_j; see Fig. 2 for an example.

4.2.3 Optimizing the Approximate Distribution

The linked-pairs crossing probability $\tilde{\mathrm{P}}_c$ computed in Eq. (11) depends on the choice of a specific spanning tree k for the vertices of c. We expect the probability to be close to the true crossing probability if the approximate multivariate distribution is similar to the original distribution. Thus, it is our aim to choose k such that the difference between the original distribution of $\mathbf{Y}$ and the approximate distribution of $\tilde{\mathbf{Y}}$ is minimal. As measure for the difference between the original and the approximate distribution, we use the Bhattacharyya distance. The Bhattacharyya distance for Gaussian distributions with identical means is given by

$$D_B(k) = \frac{1}{2}\ln\left\{\frac{\det[(\Sigma + \tilde{\Sigma}_k)/2]}{\sqrt{\det(\Sigma)\,\det(\tilde{\Sigma}_k)}}\right\}.$$

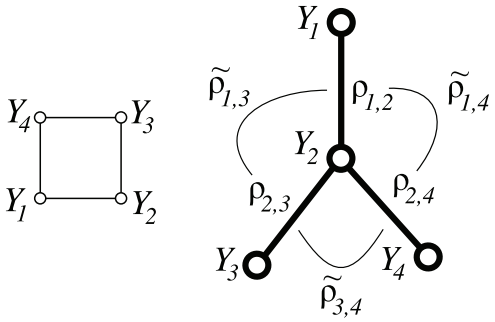

FIG. 2: One example for a spanning tree of a rectangular grid cell is shown. The choice of pairs of vertices on the edges of the tree determines the pairwise correlations that are taken from the input distribution and used to compute the remaining correlations according to Eq. (13). In this particular case $\tilde{\rho}_{1,3} = \rho_{1,2}\,\rho_{2,3}$, $\tilde{\rho}_{1,4} = \rho_{1,2}\,\rho_{2,4}$, and $\tilde{\rho}_{3,4} = \rho_{2,3}\,\rho_{2,4}$.

To obtain the optimal tree we create $\tilde{\Sigma}_k$ for all trees k enumerated by the Prüfer sequence [18], compute $D_B(k)$ and choose k_{min} such that D_B is minimal, i.e., we solve

$$k_{\text{min}} = \arg\min_k D_B(k), \tag{14}$$

and consider k_{min} in Eq. (11). The effect of the optimization is depicted in Fig. 3 where the approximation error in relation to D_B is shown.

4.2.4 Relationship to Graphical Models

Each spanning tree of a cell can also be interpreted as a *graphical model* that describes the statistical dependencies between the corresponding random variables. It contains only the connections between random variables that are present as edges in the spanning tree. The model clarifies that the variables that are *not* connected are *conditionally*

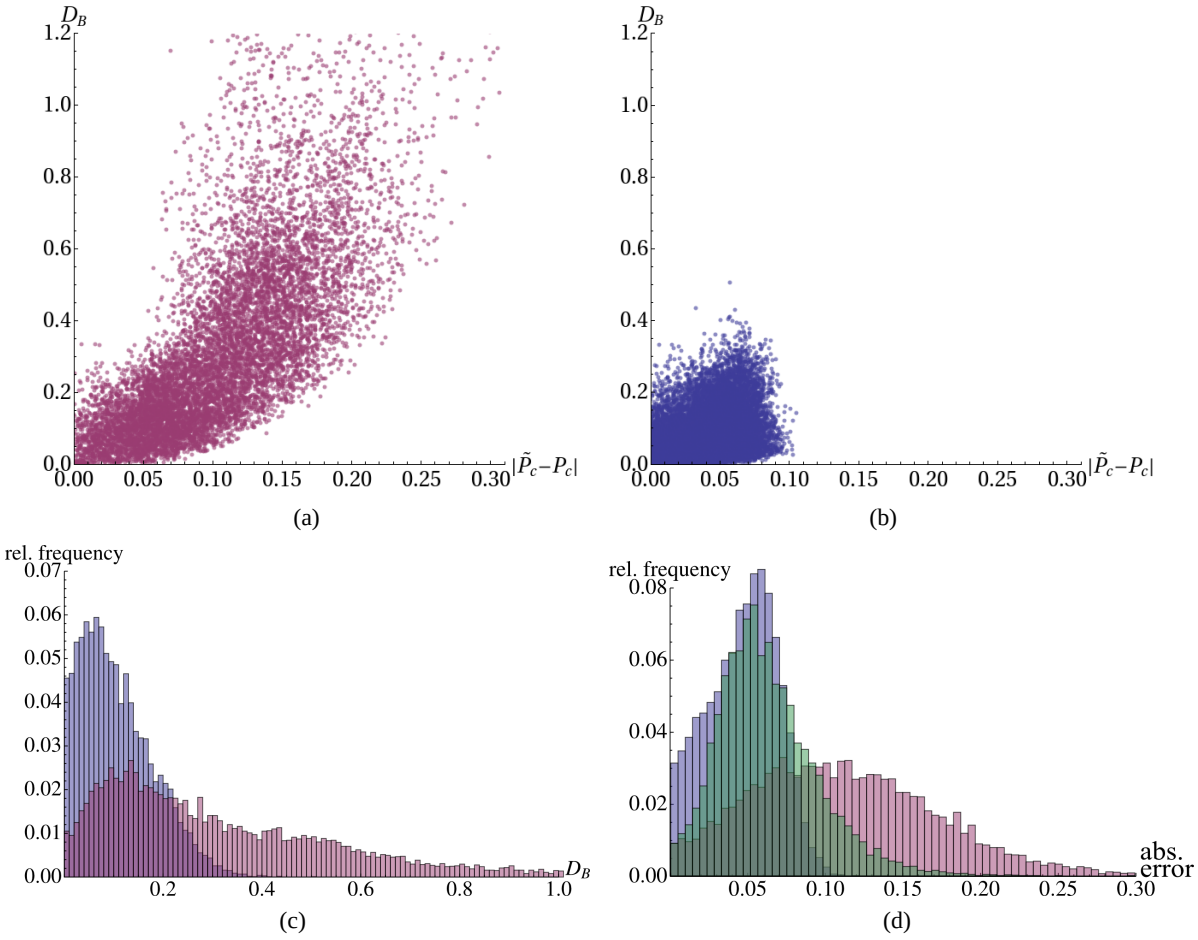

FIG. 3: Absolute approximation errors and Bhattacharyya distances for square cells with realistic covariance matrices (taken from the climate simulation data set) and expected values $\mu_i = \vartheta$ are depicted in scatter plots (a,b) and histograms (c,d). In (a) the parameter k for Eq. (10) was chosen randomly while for (b) the optimal k with minimal D_B was chosen for each cell. In (c) the histograms for D_B with (blue) and without (purple) optimal choice of k are shown. In (d), The linked-pairs approximation error with (blue) and without (purple) optimal choice of k, and the maximum edge approximation error (green) are shown.

independent in the approximate distribution. The restriction to 2D marginal distributions means that each probability can only depend on one other variable.

5. RESULTS

For a quantitative analysis of the approximation we compared the cellwise level-crossing probability P_c [Eq. (5)] that was numerically estimated using MC sampling (see [1]) to the corresponding values of the linked-pairs approximation $\tilde{P}_c$, the maximum edge crossing probability R_c, and Q_c (assuming independent vertices) for simple synthetic data sets.

The probabilities are plotted in Fig. 4 for rectangular grid cells and random vectors with constant unit variance, varying mean values in Figs. 4(a)–4(c) and varying correlation coefficient in Fig. 4(d). The cell wise probabilities P_c are drawn in blue, the approximation $\tilde{P}_c$ in magenta, R_c in green, and Q_c in yellow. The isovalue $\vartheta = 0$ is constant. In Fig. 4(a) $\mu_1 = \mu_2$ vary between -4 and 0 with constant $\mu_3 = \mu_4 = 0$. In Fig. 4(b) $\mu_1 = \mu_2 = \mu_3$ vary between -2 and 2 with $\mu_4 = -2$. In Fig. 4(c) μ_1 varies between -2 and 2 with $\mu_2 = \mu_3 = \mu_4 = -2$. In Fig. 4(d) all $\mu_i = 0$ are constant. In Fig. 4(a)–4(b) the correlation coefficient $\rho = 0.9$ is constant. In Fig. 4(d) ρ varies between 0 and 1.

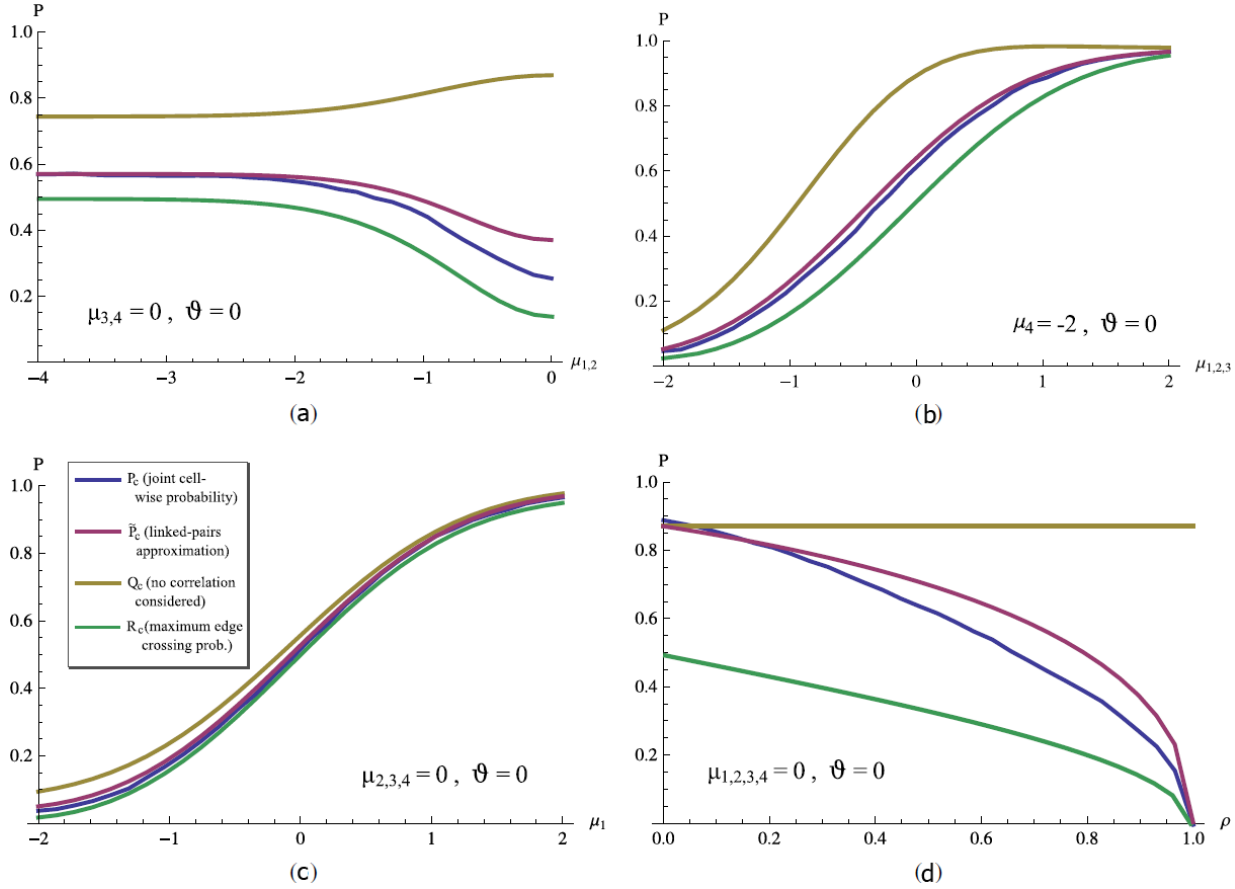

FIG. 4: (Approximate) crossing probabilities are plotted for a rectangular grid cell and random vector with constant unit variance, varying mean values in (a)–(c) and varying correlation coefficient in (d). The isovalue $\vartheta = 0$ is constant. In (a) $\mu_1 = \mu_2$ vary between -4 and 0 with constant $\mu_3 = \mu_4 = 0$. In (b) $\mu_1 = \mu_2 = \mu_3$ vary between -2 and 2 with $\mu_4 = -2$. In (c) μ_1 varies between -2 and 2 with $\mu_2 = \mu_3 = \mu_4 = -2$. In (d) all $\mu_i = 0$ are constant. In (a)–(c) the correlation coefficient $\rho = 0.9$ is constant. In (d) ρ varies between 0 and 1.

We applied the methods to a temperature field ensemble from a hindcast climate simulation of the DEMETER project [19] containing the results of seven different climate models and nine different sets of simulation parameters each. From this ensemble we estimated the mean values and covariances for all rectangular grid cells. Figure 5 depicts the correlation structure of the grid cell distributions by displaying the square roots of the eigenvalues of the correlation matrices, i.e., the standard deviations of the distribution in the spaces of their eigenvectors. Values close to 0 denote a flat distribution in the corresponding eigenvector direction, i.e., a high correlation. As depicted, correlations in the data set are on average very high in at least two eigenvector directions.

In Fig. 6 the uncertain isotherm contour for $0°\mathrm{C}$ in the temperature field from a climate simulation is displayed. Fig. 6(a) shows the crossing probabilities P_c for all pixels estimated using a MC computation with 5000 samples. Figure 6(c) shows the probabilities of the linked-pairs approximation $\tilde{\mathrm{P}}_c$ while the absolute differences, i.e., $|\tilde{\mathrm{P}}_c - \mathrm{P}_c|$, are depicted in Fig. 6(d). Analogously, the crossing probabilities Q_c assuming uncorrelated values and the difference image $|\mathrm{Q}_c - \mathrm{P}_c|$ as well as the maximum edge crossing probabilities R_c and the difference image $|\mathrm{R}_c - \mathrm{P}_c|$ are displayed. Note that the ranges of the color maps are individually adjusted for Q_c. In Fig. 6(b) the probabilities along the green line indicated in Fig. 6(a) are shown as 1D graphs.

In Fig. 7 the crossing probabilities for a 3D temperature field from the same set of climate simulations are shown. The discretized random field for this example consists of hexahedral grid cells. In Fig. 7(a) the joint cellwise crossing probabilities P_c estimated by MC sampling, (2) Q_c assuming uncorrelated values, (3) approximate probabilities $\tilde{\mathrm{P}}_c$, and (4) maximum edge crossing probabilities R_c are displayed. To allow a quantitative comparison in (5) the probabilities along a straight line in the data sets are shown as 1D graphs. The single-threaded computation times for the 3D results on an Intel i7 with 2.6 GHz are

	Time (s)
Monte Carlo integration (1000 samples/voxel)	23
Max. edge method	0.17
Linked-pairs method	0.11

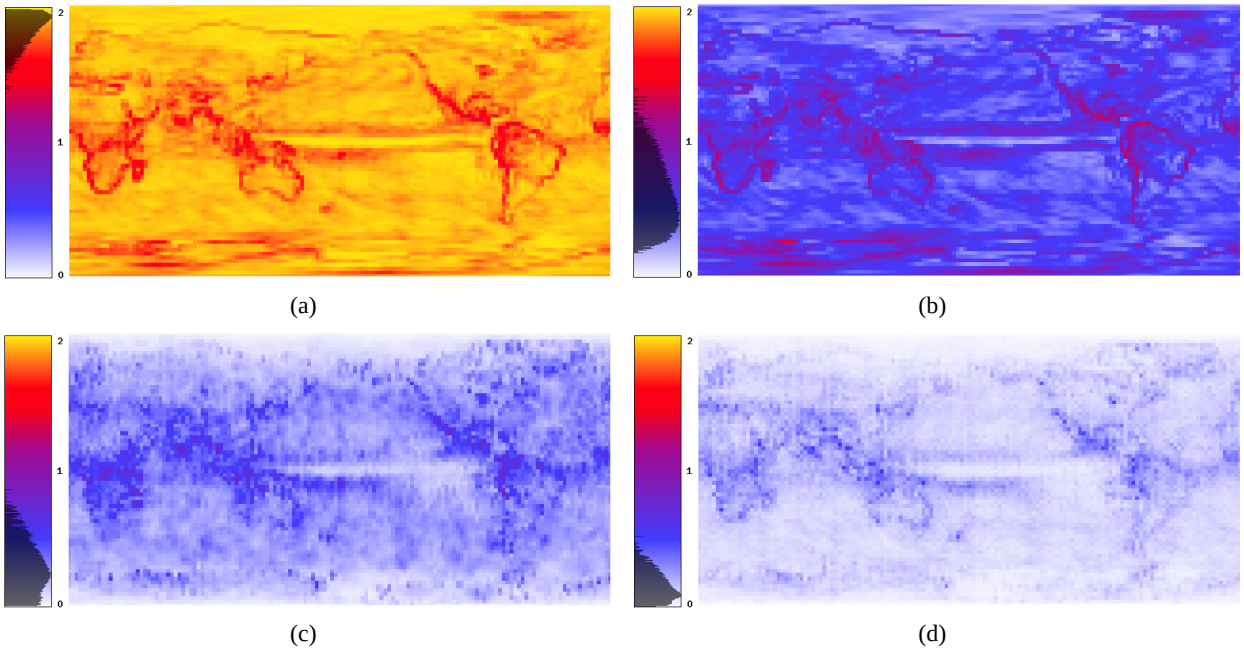

FIG. 5: Color mapped square roots of the eigenvalues (in decreasing order) of the correlation matrices of the 2D climate data set. Histograms of the values are displayed on top of the color map in logarithmic scale.

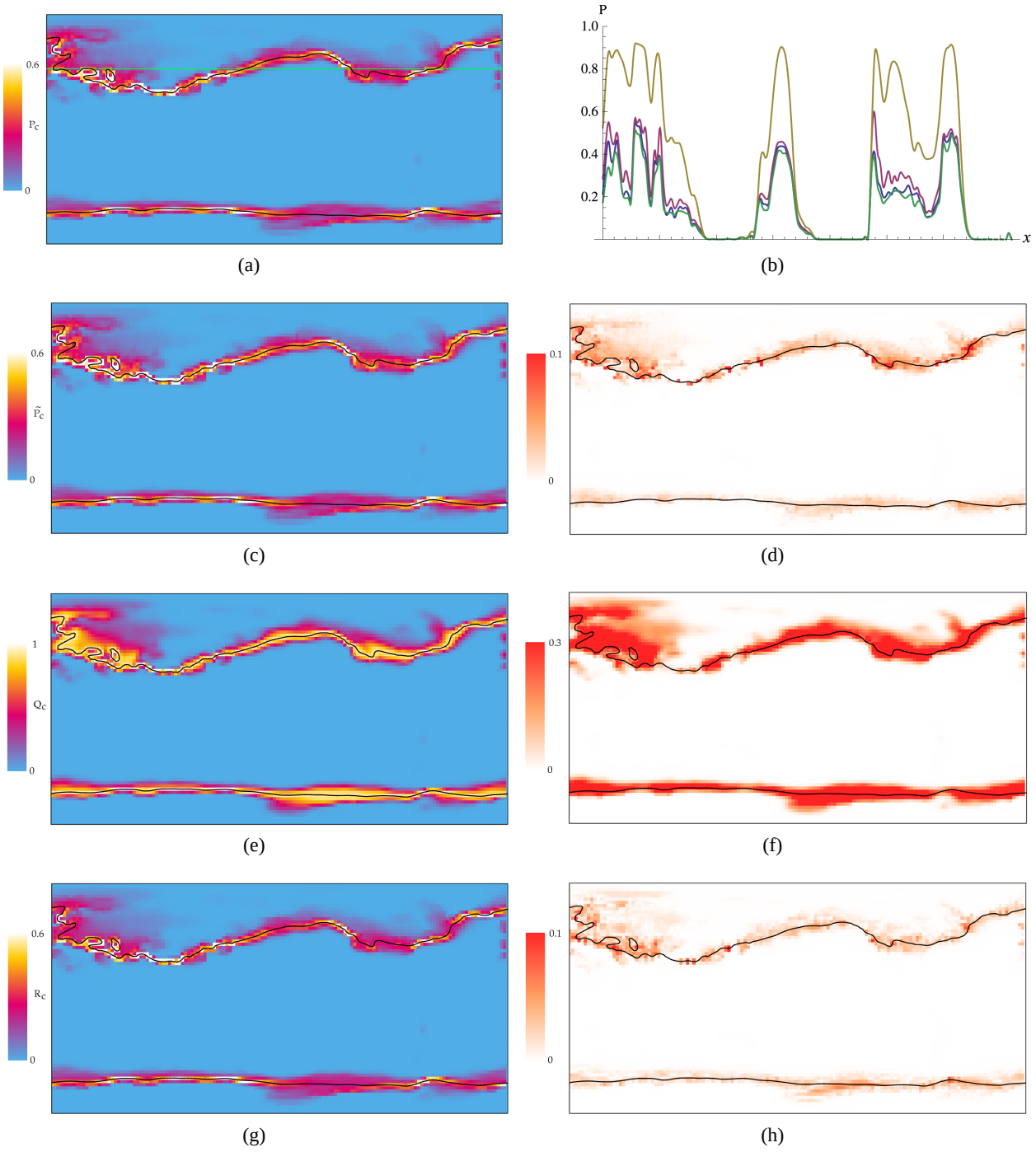

FIG. 6: Results for the 2D climate data set: (a) joint cell-wise crossing probability P_c estimated by MC sampling; (c) approximate probabilities $\tilde{\mathrm{P}}_c$; (d) difference image $|\tilde{\mathrm{P}}_c - \mathrm{P}_c|$; (e) crossing probabilities Q_c assuming uncorrelated values; (f) difference image $|\mathrm{Q}_c - \mathrm{P}_c|$; (g) maximum edge crossing probabilities R_c; (h) difference image $|\mathrm{R}_c - \mathrm{P}_c|$. Note that the ranges of the color maps are individually adjusted for Q_c. In (b) the probabilities along the green line indicated in (a) are shown as 1D graphs.

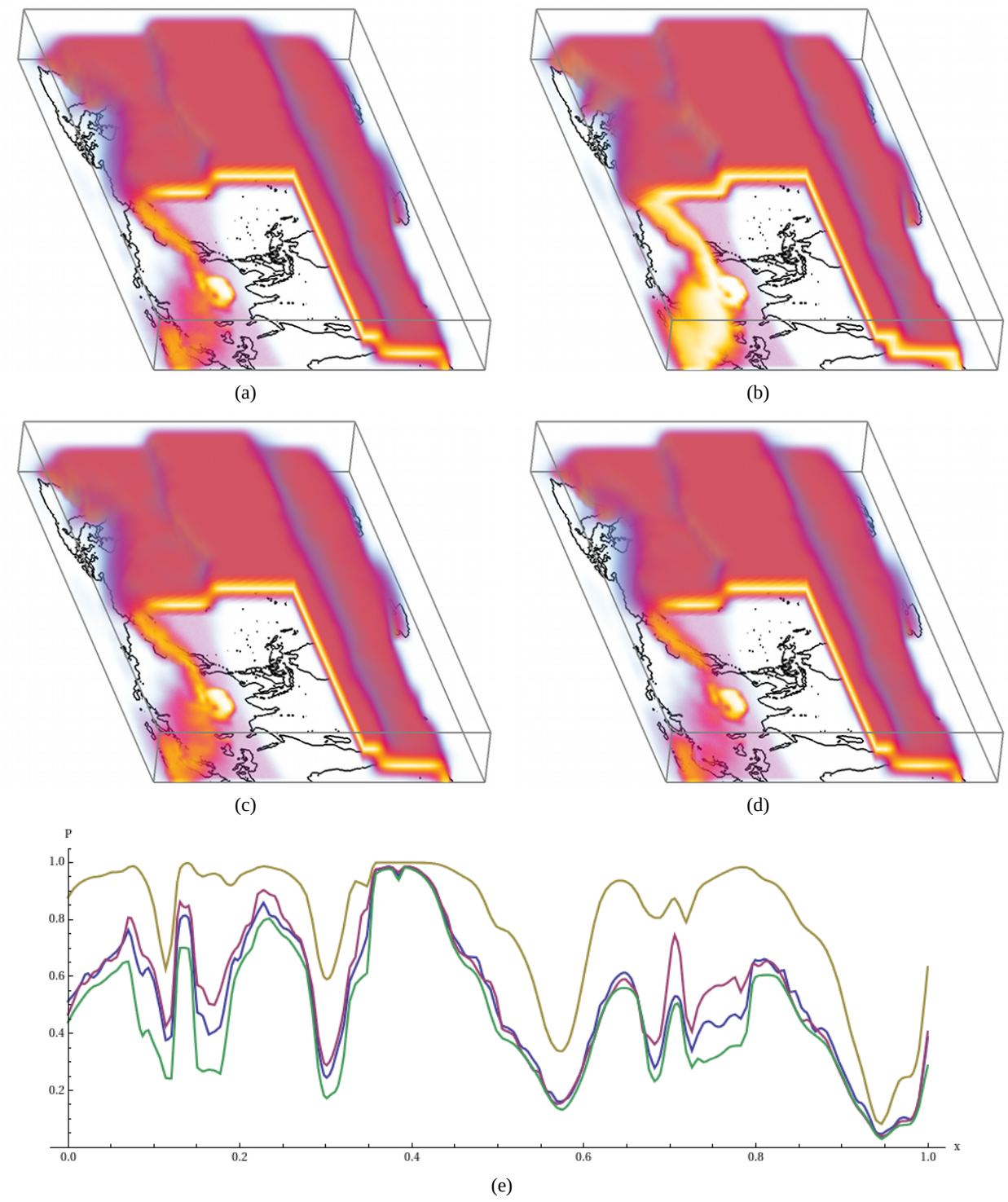

FIG. 7: Results for the 3D climate data set: (a) joint cellwise crossing probability P_c estimated by MC sampling; (b) crossing probabilities Q_c assuming uncorrelated values; (c) approximate probabilities $\tilde{\mathrm{P}}_c$; (d) maximum edge crossing probabilities R_c; In (e) the probabilities along a straight line in the data sets are shown as 1D graphs.

6. DISCUSSION

The major advantage of the approximation methods is that the crossing probabilities can be evaluated using lookup tables which results in much faster computation times compared to MC integration of the n-dimensional PDFs. Another advantage of the lookup method compared to the MC integration is that it does not suffer from MC noise.

Like Pfaffelmoser et al. [2] the approximations employ a 3D lookup table for crossing probabilities considering correlation. The motivation for their work was to develop a fast raycasting solution. Instead of local cellwise crossing probabilities they compute first-crossing probabilities along a ray which yields viewpoint-dependent results. In contrast, the results of our methods do not depend on any direction. By restricting correlation functions to the type $\exp(-|\text{distance}|)$ they could compute all probabilities along each ray. The resulting correlation coefficients corresponding to multiple pairs of random variables along a ray are similar to the covariance matrices induced by our approach to compute the approximate level-crossings using $\tilde{\mathrm{P}}_c$, i.e.; the correlation coefficients along the path are multiplied; cf. Eq. (13).

Probabilities computed with the linked-pairs approximation over- or underestimate the true level-crossing probability. In contrast, the maximum edge probability yields a true lower bound.

In Fig. 8 the volume enclosed by the semitransparent gray surfaces illustrates the space of valid correlation matrices, e.g., positive-semidefinite matrices, for three random variables. The red opaque surface depicts the result for the computed correlation in the linked-pairs approximation. The approximation over- or underestimates the real correlation. Correlation matrices that are computable with the linked-pairs approximation are located on a 2D subspace of all valid correlation matrices. The linked-pairs approximation projects the unused correlation onto that subspace. Note that the red surface depicts only one traversal order k; matrices on two additional surfaces are used in the approximation for the remaining two traversal order choices.

In the optimization step for the choice of parameter k in Eq. (10) we proposed using the Bhattacharyya distance as quality measure for the approximation. Fig. 3(a) confirms that this is a good measure, as a positive correlation

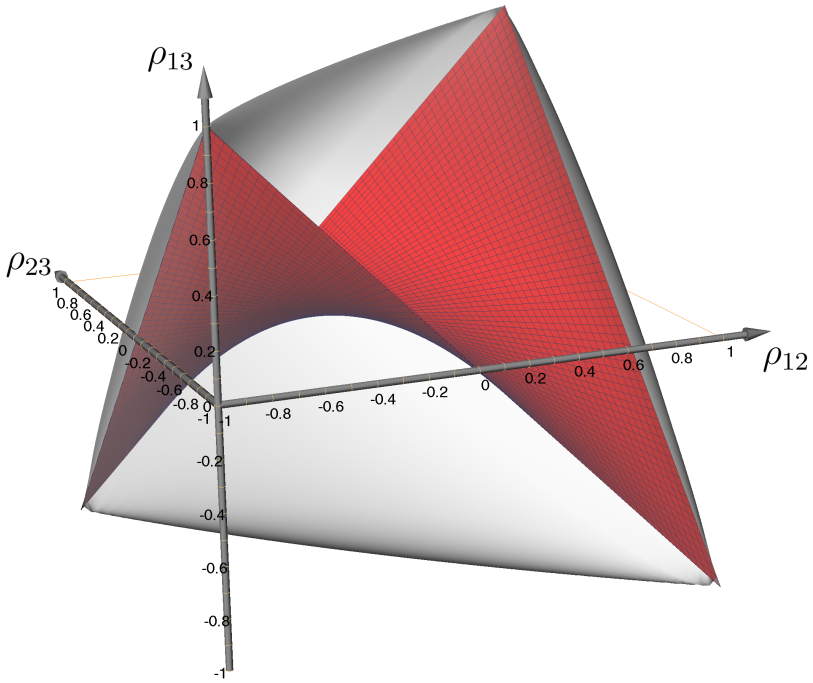

FIG. 8: Transparent gray surface encloses the space of all possible correlations between three random variables. Given the correlations between variable 1 and 2 by ρ_{12} and correlation between variable 2 and 3 by ρ_{23}, the red surface depicts the computed correlation between variables 1 and 3 in the linked-pairs approximation.

between Bhattacharyya distance D_B and approximation error exists. Choosing the optimal parameter k significantly decreases the Bhattacharyya distances and the approximation errors, as can be read off in Figs. 3(b)–4(d). In that example, the linked-pairs approximation outperforms the maximum edge approximation for optimized choice of k, but not for randomly chosen k.

Searching for the linked-pairs approximation with lowest Bhattacharyya distance as proposed in Eq. (14) requires a traversal over all spanning trees for each cell. The number of spanning trees increases with $O[\exp(N \ln N)]$, with N the number of cell vertices, what can be costly for cells with many vertices. The search is independent from a specific threshold value ϑ, and can thus be performed in a preprocessing step, allowing interactive evaluation afterwards.

A limitation of the proposed approximations is that they do not allow as to improve accuracy using a parameter or additional terms of a series expansion. As we focused on the evaluation of one- and two-dimensional distributions it is clear that we cannot reach arbitrary accuracy.

The results of the synthetic data sets in Fig. 4 and the climate data in Fig. 6 reproduce the result from previous work that spatial correlations have a significant impact on crossing probabilities. In all results the differences between P_c and Q_c are significant. In Fig. 4(a) the graph also shows qualitatively different behavior compared to the other methods.

For rectangular grid cells (2D data) (see Fig. 4), $\tilde{\mathrm{P}}_c$ overestimates P_c in most cases, while R_c underestimates it. $\tilde{\mathrm{P}}_c$ is closer to P_c; a large approximation error of R_c from P_c, up to over 0.2, can be observed in Fig. 4(d). For the climate data set, see Fig. 6. However, almost all deviations are below 0.1. The approximation of the crossing probability P_c both using $\tilde{\mathrm{P}}_c$ and the maximum edge-crossing probability R_c yields quantitatively and qualitatively good results. Visual impressions are true to the results of P_c. The 3D example yields similar results. In Fig. 7 we can observe that neglecting the correlation leads to much overestimated probabilities Q_c while $\tilde{\mathrm{P}}_c$ and R_c approximate P_c quite well.

7. CONCLUSION

We presented methods for the fast approximation of level-crossing probabilities of Gaussian random fields that allow interactive exploration of uncertain isocontours. The approximation methods reduce the computation of level-crossing probabilities to evaluations of univariate and bivariate CDFs. This is implemented using lookup tables to avoid expensive numerical integration during rendering.

In the maximum edge crossing approximation the edge-related crossing probabilities of a grid cell are computed and the maximum is taken. In the linked-pairs approximation, pairwise correlations are evaluated step by step, spanning all random variables of a cell. This induces an approximate distribution that is again normally distributed. We used the Bhattacharyya distance for choosing the optimal approximation and showed that it is a good measure for minimizing the approximation error.

Our results confirm that it is essential to consider spatial correlations. Both approximation methods, the maximum edge crossing method and the linked-pairs method, show comparable good results for real world data. While the maximum edge crossing method is conceptually simpler and provides a lower bound for real cellwise probabilities, the linked-pairs method requires a preprocessing step and—for the data sets analyzed—outperforms the maximum edge crossing method in terms of accuracy.

The approximated level-crossing probabilities are in good agreement with the true cellwise crossing probabilities, although pathological cell configurations exist where the error can be high. Experiments show that the approximation works very well in practice, and differences are hardly observable in the visualizations.

8. FUTURE WORK

Finding the optimal spanning tree in Eq. (14) is costly in the preprocessing step of the linked-pairs approximation. Contrarily, the maximum edge probability works very well in practice, and seems to select a particular edge as especially important for a cell. Using this edge as starting point for a greedy search of the optimal spanning tree potentially reduces the preprocessing effort significantly.

As proposed, original correlations between vertices of a cell are used for the linked-pairs approximation. It might be possible to further reduce the Bhattacharyya distance of the approximated distribution by relaxing this requirement

and distribute correlation deviations among all entries of the correlation matrix. Preliminary experiments indicate that the Bhattacharyya distance can further be reduced with an additional simple gradient-based optimization method.

APPENDIX

In the following, we show that the approximate distribution for $\tilde{\mathbf{Y}}$ is again a multivariate normal distribution, and derive a formula for computing the covariance matrix of that approximate distribution. Without loss of generality, distributions with zero mean are assumed. Pairwise correlations are iteratively added to a multivariate distribution, yielding again another multivariate distribution that serves as input for the next step. By reordering random variables, we always extend the last variable of a random vector.

Given a n-dimensional multivariate normal distribution of the random vector $\mathbf{Y} = [Y_1, Y_2, \ldots, Y_n]$ with covariance matrix $\Sigma = (\rho_{ij}\sigma_i\sigma_j)_{1\leq i,j\leq n}$, variances σ_i^2 and $\rho_{ii} = 1$, we consider a second random vector $\bar{\mathbf{Y}} = [Y_n, Y_{n+1}]$ with a two-dimensional normal distribution that describes the extension of $\mathbf{Y}$ by another variable. The covariance matrix of $\bar{\mathbf{Y}}$ is

$$\Sigma_{\bar{\mathbf{Y}}} = \begin{pmatrix} \sigma_n^2 & \rho_{n,n+1}\sigma_n\sigma_{n+1} \\ \rho_{n,n+1}\sigma_n\sigma_{n+1} & \sigma_{n+1}^2 \end{pmatrix}. \tag{15}$$

Covariances between the first $n-1$ variables and $n+1$ are not explicitly stated. In the following, the PDF of the joint distribution of the two distributions is computed.

With $f_{\mathbf{Y}}(y_1, \ldots, y_n)$, the PDF describing $\mathbf{Y}$, and $f_{y_{n+1}}(y_{n+1}|y_n)$ the PDF of the conditional distribution of y_{n+1} given y_n, the joint PDF is given by the product of both PDFs, as $f_{y_{n+1}}$ is independent from $y_1 \ldots y_{n-1}$:

$$f(y_1, \ldots, y_{n+1}) = f_{\mathbf{Y}}(y_1, \ldots, y_n) f_{y_{n+1}}(y_{n+1}|y_n) \tag{16}$$

The n-dimensional multivariate normal distribution is given by

$$f_{\mathbf{Y}}(y_1, \ldots, y_n) = \frac{1}{(2\pi)^{n/2}\,|\Sigma|^{1/2}} \exp\left[-\frac{1}{2}(y_1 \ldots y_n)\Sigma^{-1}(y_1 \ldots y_n)^T\right] \tag{17}$$

The conditional density for y_{n+1} given y_n is again normally distributed with mean $\bar{\mu} = \alpha y_n$, where $\alpha = \rho_{n,n+1}\frac{\sigma_{n+1}}{\sigma_n}$ and variance $\bar{\sigma}^2 = \sigma_{n+1}^2(1-\rho_{n,n+1}^2)$. It is then

$$f_{y_{n+1}}(y_{n+1}|y_n) = \frac{1}{\sqrt{2\pi\bar{\sigma}^2}} \exp\left[-\frac{(y_{n+1}-\alpha y_n)^2}{2\bar{\sigma}^2}\right], \tag{18}$$

and can be written in matrix form as

$$f_{y_{n+1}}(y_{n+1}|y_n) = \frac{1}{\sqrt{2\pi\bar{\sigma}^2}} \exp\left[-\frac{1}{2}(y_n y_{n+1}) \begin{pmatrix} \alpha^2/\bar{\sigma}^2 & -\alpha/\bar{\sigma}^2 \\ -\alpha/\bar{\sigma}^2 & 1/\bar{\sigma}^2 \end{pmatrix} \begin{pmatrix} y_n \\ y_{n+1} \end{pmatrix}\right]. \tag{19}$$

Using the following identity for the inverse of the $(n+1)\times(n+1)$ matrix and employing block matrix notation

$$\left[\begin{pmatrix} \Sigma^{-1} & 0 \\ & \vdots \\ 0 & \cdots \quad 0 \end{pmatrix} + \begin{pmatrix} 0 & \cdots & 0 & 0 & 0 \\ \vdots & \ddots & \vdots & \vdots & \vdots \\ 0 & \cdots & 0 & 0 & 0 \\ 0 & \cdots & 0 & \alpha^2/\bar{\sigma}^2 & -\alpha/\bar{\sigma}^2 \\ 0 & \cdots & 0 & -\alpha/\bar{\sigma}^2 & 1/\bar{\sigma}^2 \end{pmatrix}\right]^{-1} = \begin{pmatrix} \Sigma & \alpha\Sigma_n \\ \alpha\Sigma_n^T & \alpha^2\Sigma_{n,n} + \bar{\sigma}^2 \end{pmatrix},$$

where Σ_n is the nth column of Σ and $\Sigma_{n,n}$ the entry at (n,n) of Σ, the joint distribution f can be written as

$$f(y_1, \ldots y_{n+1}) = \frac{1}{(2\pi)^{\frac{n+1}{2}}\,|\Sigma|^{\frac{1}{2}}\,|\bar{\sigma}^2|^{\frac{1}{2}}} \exp\left[-\frac{1}{2}(y_1 \ldots y_{n+1}) \begin{pmatrix} \Sigma & \alpha\Sigma_n \\ \alpha\Sigma_n^T & \alpha^2\Sigma_{n,n} + \bar{\sigma}^2 \end{pmatrix}^{-1} \begin{pmatrix} y_1 \\ \vdots \\ y_{n+1} \end{pmatrix}\right]. \tag{20}$$

With $\alpha^2\Sigma_{n,n} + \bar{\sigma}^2 = \sigma_{n+1}^2$ and

$$\Sigma^* = \begin{pmatrix} \Sigma & \alpha\Sigma_n \\ \alpha\Sigma_n^T & \sigma_{n+1}^2 \end{pmatrix} \tag{21}$$

the joint distribution is finally

$$f(y_1, \dots y_{n+1}) = \frac{1}{(2\pi)^{\frac{n+1}{2}} |\Sigma^*|^{\frac{1}{2}}} \exp\left[-\frac{1}{2}(y_1 \dots y_{n+1})\Sigma^{*-1}(y_1 \dots y_{n+1})^T\right]. \tag{22}$$

It is left to show that $|\Sigma\bar{\sigma}^2| = |\Sigma^*|$. Applying the block matrix formula for determinants

$$\left|\begin{pmatrix} A & B \\ C & D \end{pmatrix}\right| = |A||D - CA^{-1}B| \tag{23}$$

to Eq. (21) yields the desired equality:

$$\begin{aligned} |\Sigma^*| &= |\Sigma||\sigma_{n+1}^2 - \alpha\Sigma_n^T\Sigma^{-1}\alpha\Sigma_n| \\ &= |\Sigma||\sigma_{n+1}^2 - \alpha^2\Sigma_n^T(0 \cdots 01)^T| \\ &= |\Sigma||\sigma_{n+1}^2 - \alpha^2\Sigma_{nn}| \\ &= |\Sigma||\sigma_{n+1}^2 - \alpha^2\sigma_n^2| \\ &= |\Sigma||\sigma_{n+1}^2(1 - \rho_{n,n+1}^2)| \\ &= |\Sigma||\bar{\sigma}^2| \\ &= |\Sigma\bar{\sigma}^2|. \end{aligned} \tag{24}$$

The last column of Eq. (21) contains the covariances between $Y_1, \cdots Y_n$ and the last variable Y_{n+1}. The covariances are

$$\alpha\Sigma_N = (\rho_{i,n}\rho_{n,n+1}\sigma_i\sigma_{n+1})_{1 \le i \le n}, \tag{25}$$

i.e., the correlations to variable Y_n are multiplied by $\rho_{n,n+1}$ for variable Y_{n+1}.

REFERENCES

1. Pöthkow, K., Weber, B., and Hege, H.-C., Probabilistic marching cubes, *Comput. Graphics Forum*, 30(3):931–940, 2011.
2. Pfaffelmoser, T., Reitinger, M., and Westermann, R., Visualizing the positional and geometrical variability of isosurfaces in uncertain scalar fields, *Comput. Graphics Forum*, 30(3):951–960, 2011.
3. Johnson, C. R. and Sanderson, A. R., A next step: Visualizing errors and uncertainty, *IEEE Comput. Graphics Appl.*, 23(5):6–10, 2003.
4. Pang, A. T., Wittenbrink, C. M., and Lodha, S. K., Approaches to uncertainty visualization, *Visual Comput.*, 13(8):370–390, 1997.
5. Potter, K., Wilson, A., Bremer, P.-T., Williams, D., Doutriaux, C., Pascucci, V., and Johhson, C. R., Ensemble-Vis: A framework for the statistical visualization of ensemble data, In *Proc. of IEEE Workshop on Knowledge Discovery from Climate Data: Prediction, Extremes*, pp. 233–240, 2009.
6. Sanyal, J., Zhang, S., Dyer, J., Mercer, A., Amburn, P., and Moorhead, R., Noodles: A tool for visualization of numerical weather model ensemble uncertainty, *IEEE Trans. Visualization Comput. Graphics*, 16:1421–1430, 2010.
7. Luo, A., Kao, D., and Pang, A., Visualizing spatial distribution data sets, In *VISSYM '03: Proc. of the Symposium on Data Visualization*, Eurographics Association, pp. 29–38, 2003.
8. Djurcilov, S., Kim, K., Lermusiaux, P., and Pang, A., Visualizing scalar volumetric data with uncertainty, *Comput. Graphics*, 26(2):239–248, 2002.
9. Kniss, J. M., Uitert, R. V., Stephens, A., Li, G.-S., Tasdizen, T., and Hansen, C., Statistically quantitative volume visualization, In *Proc. of IEEE Visualization*, pp. 287–294, 2005.

10. Lundström, C., Ljung, P., Persson, A., and Ynnerman, A., Uncertainty visualization in medical volume rendering using probabilistic animation, *IEEE Trans. Visualization Comput. Graphics*, 13(6):1648–1655, 2007.
11. Botchen, R. P., Weiskopf, D., and Ertl, T., Texture-based visualization of uncertainty in flow fields, In *Proc. of IEEE Visualization*, New York, IEEE, pp. 647–654, 2005.
12. Otto, M., Germer, T., Hege, H.-C., and Theisel, H., Uncertain 2D vector field topology, *Comput. Graphics Forum*, 29:347–356, 2010.
13. Pauly, M., Mitra, N., and Guibas, L., Uncertainty and variability in point cloud surface data, In *Proc. of Eurographics Symposium on Point-Based Graphics*, pp. 77–84, 2004.
14. Grigoryan, G. and Rheingans, P., Point-based probabilistic surfaces to show surface uncertainty, *IEEE Trans. Visualization Comput. Graphics*, 10(5):564–573, 2004.
15. Zehner, B., Watanabe, N., and Kolditz, O., Visualization of gridded scalar data with uncertainty in geosciences, *Comput. Geosci.*, 36(10):1268–1275, 2010.
16. Allendes Osorio, R. and Brodlie, K., Contouring with uncertainty, In: Lim, I. S. and Tang, W. Eds., *Theory and Practice of Computer Graphics—Eurographics UK Chapter Proceedings*, pp. 59–66, Eurographics Association, 2008.
17. Pöthkow, K. and Hege, H.-C., Positional uncertainty of isocontours: Condition analysis and probabilistic measures, *IEEE Trans. Visualization Comput. Graphics*, 17(10):1393–1406, 2011.
18. Prüfer, H., Neuer Beweis eines Satzes über Permutationen, *Arch. Math. Phys.*, 27:742–744, 1918.
19. Palmer, T. N., Doblas-Reyes, F. J., Hagedorn, R., Alessandri, A., Gualdi, S., Andersen, U., Feddersen, H., Cantelaube, P., Terres, J.-M., Davey, M., Graham, R., Délécluse, P., Lazar, A., M. Déqué, J.-F. G., Díez, E., Orfila, B., Hoshen, M., Morse, A. P., Keenlyside, N., Latif, M., Maisonnave, E., Rogel, P., Marletto, V., and Thomson, M. C., Development of a European multimodel ensemble system for seasonal to inter-annual prediction (DEMETER), *Bull. Am. Meteorol. Soc.*, 85(6):853–872, 2004.